

# Imaging of K<sub>Ca</sub>3.1 Channels in Tumor Cells with PET and Small-Molecule Fluorescent Probes

Insa Thale,<sup>[a, b]</sup> Sarah Maskri,<sup>[a, b]</sup> Lucie Grey,<sup>[b]</sup> Luca Matteo Todesca,<sup>[a, c]</sup> Thomas Budde,<sup>[a, d]</sup> Ivan Maisuls,<sup>[e, f]</sup> Cristian A. Strassert,<sup>[e, f]</sup> Oliver Koch,<sup>[a, b]</sup> Albrecht Schwab,<sup>[a, c]</sup> and Bernhard Wünsch<sup>\*[a, b]</sup>

The Ca<sup>2+</sup> activated K<sup>+</sup> channel K<sub>Ca</sub>3.1 is overexpressed in several human tumor cell lines, e.g. clear cell renal carcinoma, prostate cancer, non-small cell lung cancer. Highly aggressive cancer cells use this ion channel for key processes of the metastatic cascade such as migration, extravasation and invasion. Therefore, small molecules, which are able to image this K<sub>Ca</sub>3.1 channel *in vitro* and *in vivo* represent valuable diagnostic and prognostic tool compounds. The [<sup>18</sup>F]fluoroethyltriazolyl substituted senicapoc was used as positron emission tomography (PET) tracer and showed promising properties for imaging of K<sub>Ca</sub>3.1 channels in lung adenocarcinoma cells in mice. The novel senicapoc BODIPY conjugates with two F-atoms (**9a**) and with a

F-atom and a methoxy moiety (**9b**) at the B-atom led to the characteristic punctate staining pattern resulting from labeling of single K<sub>Ca</sub>3.1 channels in A549-3R cells. This punctate pattern was completely removed by preincubation with an excess of senicapoc confirming the high specificity of K<sub>Ca</sub>3.1 labeling. Due to the methoxy moiety at the B-atom and the additional oxyethylene unit in the spacer, **9b** exhibits higher polarity, which improves solubility and handling without reduction of fluorescence quantum yield. Docking studies using a cryo-electron microscopy (EM) structure of the K<sub>Ca</sub>3.1 channel confirmed the interaction of **9a** and **9b** with a binding pocket in the channel pore.

## Introduction

### K<sub>Ca</sub>3.1 channel

The Ca<sup>2+</sup>-activated K<sup>+</sup> channel 3.1 (K<sub>Ca</sub>3.1) also known as Garlos channel, I<sub>KCa</sub> channel or SK4 channel belongs to the heterogeneous family of K<sup>+</sup> channels which are activated by intracellular Ca<sup>2+</sup> ions.<sup>[1]</sup> The K<sub>Ca</sub>3.1 channel is formed by the assembly of four identical subunits (homotetramer), which are encoded by the *KCNN4* gene. Each subunit consists of six transmembrane helices and both the amino and carboxy termini are located at the cytosolic side of the membrane. The ion channel pore is located between the 5<sup>th</sup> and 6<sup>th</sup> transmembrane helix.<sup>[2]</sup> The K<sub>Ca</sub>3.1 channel possesses a calmodulin binding site, which is

located intracellularly in the C-terminus close to the membrane.<sup>[3,4]</sup>

K<sub>Ca</sub>3.1 channels are widely expressed in many human tissues and organs. It is highly expressed in secretory epithelial cells such as those of the gastrointestinal tract and the pancreas.<sup>[5,6,7]</sup> Moreover, essentially all blood cells and microglial cells express the K<sub>Ca</sub>3.1 channel, where it contributes to migration, activation and cytokine release.<sup>[8,9]</sup> Due to its widespread distribution, dysregulation of the K<sub>Ca</sub>3.1 channel was observed in various inflammatory neurological disorders, e.g. ischemic stroke, epilepsy, Alzheimer's disease, Multiple sclerosis,<sup>[10–14]</sup> and vascular diseases (e.g. kidney fibrosis,<sup>[15,16]</sup> atherosclerosis,<sup>[17,18]</sup> and restenosis).<sup>[19,20]</sup>

[a] I. Thale, S. Maskri, L. M. Todesca, Prof. Dr. T. Budde, Prof. Dr. O. Koch, Prof. Dr. A. Schwab, Prof. Dr. B. Wünsch  
Westfälische Wilhelms-Universität Münster  
GRK 2515

Chemical biology of ion channels (Chembion)  
Corrensstraße 48, 48149 Münster (Germany)


[b] I. Thale, S. Maskri, L. Grey, Prof. Dr. O. Koch, Prof. Dr. B. Wünsch  
Westfälische Wilhelms-Universität Münster  
Institut für Pharmazeutische und Medizinische Chemie  
Corrensstraße 48, 48149 Münster (Germany)  
E-mail: wuensch@uni-muenster.de


[c] L. M. Todesca, Prof. Dr. A. Schwab  
Westfälische Wilhelms-Universität Münster  
Universitätsklinikum Münster  
Institute of Physiology II  
Robert-Koch-Straße 27b, 48149 Münster (Germany)

[d] Prof. Dr. T. Budde  
Westfälische Wilhelms-Universität Münster  
Universitätsklinikum Münster  
Institute of Physiology I  
Robert-Koch-Straße 27a, 48149 Münster (Germany)

[e] Dr. I. Maisuls, Prof. Dr. C. A. Strassert  
Westfälische Wilhelms-Universität Münster  
Institut für Anorganische und Analytische Chemie  
CiMIC, SoN  
Corrensstraße 28, 48149 Münster (Germany)

[f] Dr. I. Maisuls, Prof. Dr. C. A. Strassert  
Westfälische Wilhelms-Universität Münster  
CeNTech  
Heisenbergstraße 11, 48149, Münster (Germany)

 Supporting information for this article is available on the WWW under <https://doi.org/10.1002/cmdc.202200551>

 © 2022 The Authors. ChemMedChem published by Wiley-VCH GmbH. This is an open access article under the terms of the Creative Commons Attribution Non-Commercial License, which permits use, distribution and reproduction in any medium, provided the original work is properly cited and is not used for commercial purposes.

Several human cancer cells such as clear cell renal cell carcinoma (ccRCC),<sup>[21]</sup> papillary thyroid cancer (PTC),<sup>[22]</sup> human prostate cancer,<sup>[23]</sup> non-small cell lung cancer (NSCLC)<sup>[24,25]</sup> as well as breast cancer cells MCF-7<sup>[26]</sup> express high amounts of K<sub>Ca</sub>3.1 channels. In NSCLC patients the hypomethylation of the K<sub>Ca</sub>3.1 channel promoter, which in turn is responsible for its elevated expression, is a strong predictor of poor patient prognosis.<sup>[25]</sup> Highly aggressive cancer cells require the K<sub>Ca</sub>3.1 channel for key processes of the metastatic cascade including migration, extravasation and invasion<sup>[27,28]</sup> as well as for proliferation<sup>[29]</sup> and development of resistance (e.g. against irradiation, cisplatin or EGFR tyrosine kinase inhibitor erlotinib).<sup>[30–32]</sup> One important function of K<sub>Ca</sub>3.1 channels is to hyperpolarize the cell membrane potential thereby providing a favorable driving force for the influx of Ca<sup>2+</sup> ions into the cell. The increased intracellular Ca<sup>2+</sup> concentration allows the cells among others to pass the G<sub>0</sub>/G<sub>1</sub> and G<sub>1</sub>/S checkpoints resulting in increased cell proliferation. Based on the multiple functions of K<sub>Ca</sub>3.1 channels in tumor and tumor stroma cells they may represent a promising target for the treatment of cancer.<sup>[28]</sup>

It was found that the antifungal drug clotrimazole (1, Figure 1) inhibits the K<sub>Ca</sub>3.1 channel. Treatment of mice transplanted with human endometrial cancer cells with clotrimazole led to reduced mass of the tumor. The same effect was observed upon treatment with the clotrimazole analog TRAM-34 (2).<sup>[33]</sup> TRAM-34 contains a pyrazole ring instead of the imidazole ring of clotrimazole, which reduces the interactions with Fe<sup>3+</sup> containing enzymes, such as CYP enzymes. Another similarly effective K<sub>Ca</sub>3.1 channel inhibitor is senicapoc (3). It was originally tested for the treatment of sickle cell anemia<sup>[34]</sup> and also led to decreased tumor mass after treatment of mice bearing the non-small cell lung cancer cells A549-3R.<sup>[25]</sup>

In addition to the tumor itself, stroma cells in the micro-environment of the tumor, such as immune cells, cancer-associated fibroblasts and endothelial cells, play a crucial role for remodeling of the tumor microenvironment and tumor growth. It was shown that immune cells in the stroma overexpress the K<sub>Ca</sub>3.1 channel and release K<sup>+</sup> ions leading to restore T-cell function and reduce tumor proliferation.<sup>[35,36]</sup>

### Imaging of the K<sub>Ca</sub>3.1 channel by positron emission tomography (PET)

The metastatic status and the aggressiveness of a tumor often correlate with the density/expression of K<sub>Ca</sub>3.1 channels in the tumor, but also in its stroma.<sup>[37]</sup> K<sub>Ca</sub>3.1 channel expression was used as predictive biomarker for the localization of a tumor and for the prognosis of the disease. Positron emission tomography (PET) allows for imaging of targets *in vivo*. The K<sub>Ca</sub>3.1 channel represents a promising target to be addressed by PET, as almost all cells of the tumor and tumor stroma express this ion channel.<sup>[37]</sup> Therefore, a strong signal is expected by a PET tracer labeling K<sub>Ca</sub>3.1 channels.

For the development of a PET tracer, the K<sub>Ca</sub>3.1 channel inhibitor senicapoc (3) was used as lead compound. It binds with high affinity at the K<sub>Ca</sub>3.1 channel (IC<sub>50</sub> = 11 nM) and shows excellent selectivity over related ion channels.<sup>[38]</sup> Since senicapoc (3) has already been used in human clinical trials for the treatment of sickle cell anemia,<sup>[28,38]</sup> it represents an ideal starting point for the development of imaging probes.

At first, the fluorinated PET tracer [<sup>18</sup>F]5 was designed for *in vivo* imaging of the K<sub>Ca</sub>3.1 channel. (Scheme 1) For this purpose, the tosylate precursor 4 was transformed into [<sup>18</sup>F]5 by a nucleophilic substitution with [<sup>18</sup>F]fluoride. After optimization of the radiosynthesis, biodistribution studies were performed with [<sup>18</sup>F]5. Unfortunately, high activity uptake by the bones was observed, which indicated the release of [<sup>18</sup>F]fluoride from the PET tracer.<sup>[39]</sup>

Based on the results with the PET tracer [<sup>18</sup>F]5, the fluoroethyltriazole [<sup>18</sup>F]7 was designed as second generation PET tracer. (Scheme 1) A copper-catalyzed 1,3-dipolar cyclo-addition of alkyne precursor 6 with *in situ* prepared [<sup>18</sup>F]fluoroethyl azide provided the triazole [<sup>18</sup>F]7 in good radiochemical yields and purity. In patch clamp experiments the non-radioactive triazole 7 was able to inhibit and thus to bind to the K<sub>Ca</sub>3.1 channel. [<sup>18</sup>F]7 was stable in mouse and human serum. Biodistribution studies showed a clean profile with fast elimination of the radioactivity via kidney and liver. Therefore, [<sup>18</sup>F]7 was employed in a tumor model. A549-3R lung adenocarcinoma cells expressing high density of the K<sub>Ca</sub>3.1

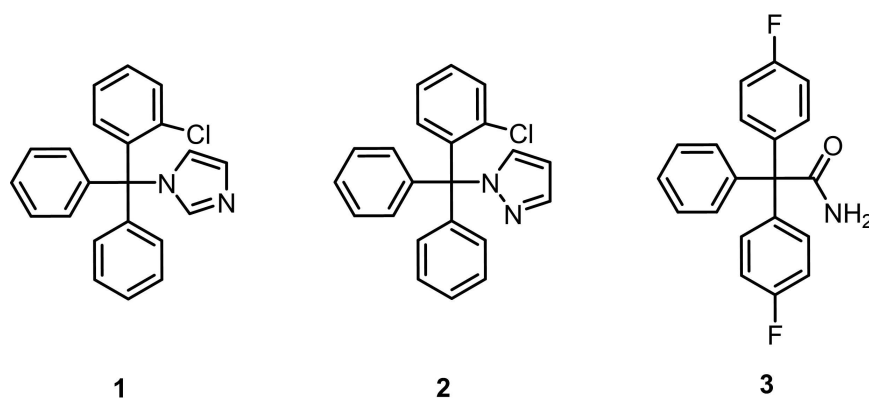
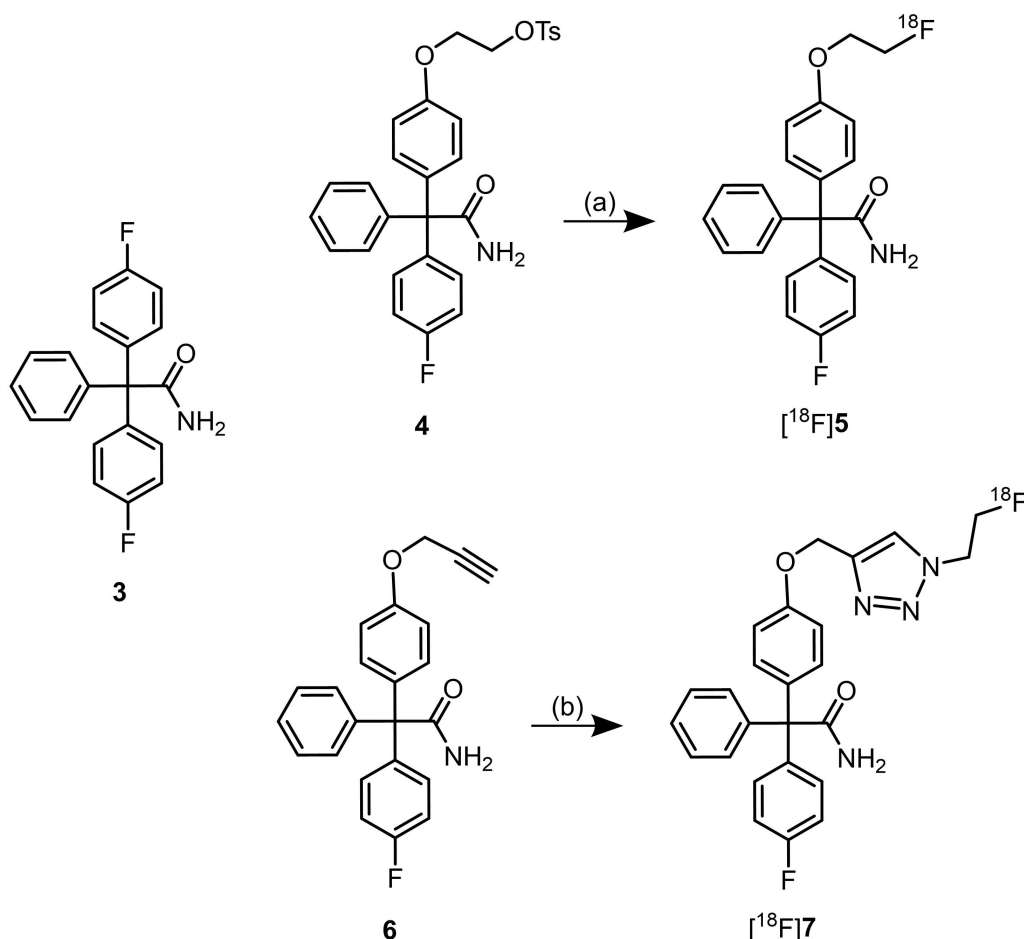


**Figure 1.** Prominent inhibitors of the K<sub>Ca</sub>3.1 channel: the antifungal drug clotrimazole (1) represents the first member of this class of K<sub>Ca</sub>3.1 channel blockers, which was developed into TRAM-34 (2) and senicapoc (3).



**Scheme 1.** Senicapoc (**3**) and senicapoc derived fluorinated PET tracers. Reactions and reaction conditions: (a)  $[^{18}\text{F}]\text{KF}$ , K222,  $\text{CH}_3\text{CN}$ ,  $90^\circ\text{C}$ , 15 min, radiochemical yield (decay corrected)  $4 \pm 1.5\%$ .<sup>[39]</sup> (b) 1.  $\text{N}_3\text{CH}_2\text{CH}_2\text{OTs} + [^{18}\text{F}]\text{KF}$ , K222,  $\text{CH}_3\text{CN}$ ,  $110^\circ\text{C}$ , 3 min, distillation under helium flow; 2. prepared  $\text{N}_3\text{CH}_2\text{CH}_2^{18}\text{F} + \mathbf{6}$ ,  $\text{CuSO}_4$ , sodium ascorbate,  $\text{H}_2\text{O}$ , DMF  $60^\circ\text{C}$ , 30 min. radiochemical yield (decay corrected)  $13 \pm 4.6\%$ , over two steps.<sup>[40]</sup>

channel, were implanted subcutaneously. The fluorinated PET tracer  $[^{18}\text{F}]\mathbf{7}$  showed considerable tumor uptake, but moderate tumor-to-muscle ratios. The moderate tumor-to-muscle ratio may be due to the wide expression of the targeted  $\text{K}_{\text{Ca}3.1}$  channel.<sup>[40]</sup>

### Imaging of the $\text{K}_{\text{Ca}3.1}$ channel by small-molecule fluorescent probes

A fluorescent probe, which is able to label selectively  $\text{K}_{\text{Ca}3.1}$  channels, represents a valuable tool to detect cells with high density of the ion channel. Compared to labeling with antibodies, *in vitro* staining with fluorescent probes is cheap, simple, efficient and fast (ca. 10–20 min). Moreover, optimized fluorescent probes with appropriate fluorescent dyes could be used for *in vivo* imaging as well.

In general, a fluorescent probe designed to label the  $\text{K}_{\text{Ca}3.1}$  channel has to contain a targeting unit (“warhead”) connected via a linker with a fluorescent dye. Senicapoc was selected as warhead and BODIPY as fluorescent dye. Both components had

to be connected by an appropriate linker in an appropriate position. (Figure 2)

In a previous study, senicapoc was connected with a BODIPY dye via a 1,3-dipolar cycloaddition. The resulting probe **8** showed very good imaging properties, allowing the visualization of single  $\text{K}_{\text{Ca}3.1}$  channels of aggressive non-small cell lung cancer cells A549-3R. Incubation of the cells with the BODIPY-labeled senicapoc derivative **8** for a period of only 10 min led to the typical punctate staining pattern, which could be blocked by pre-incubation with senicapoc. The density of  $\text{K}_{\text{Ca}3.1}$  channels determined by direct staining with **8** was identical with the density obtained by antibody-based indirect immunofluorescence.<sup>[41,42]</sup>

## Results and Discussion

### Design, of polar fluorescent probes to image the $\text{K}_{\text{Ca}3.1}$ channel

As the binding site of senicapoc is located within the ion channel, it is hypothesized that the fluorescent probe has to

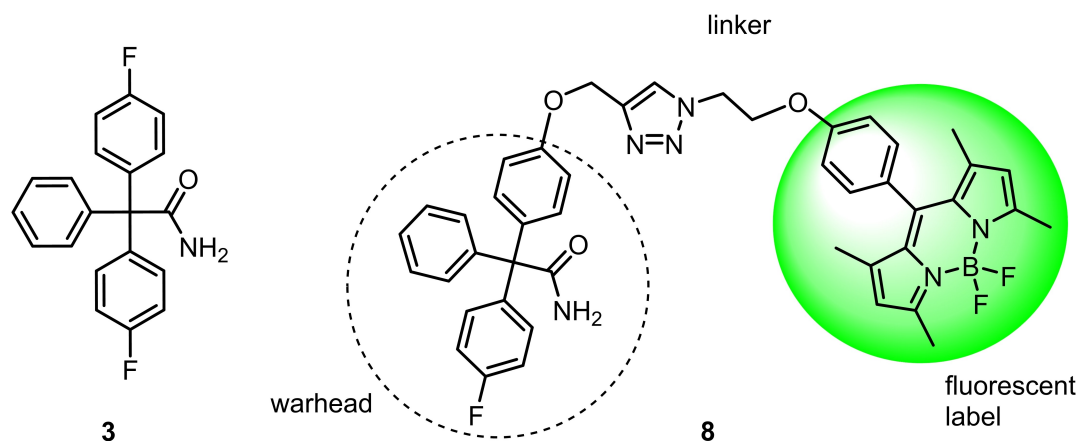


**Figure 2.** The fluorescent probe **8** consists of a senicapoc warhead (targeting unit) connected via a linker with a fluorescent label.

penetrate into the cell and enter the ion channel from the inside of the channel pore. For this purpose, the dye should possess well-balanced lipophilic properties allowing it to penetrate the membrane but not to stick in the membrane. Since the probe **8** is rather lipophilic, we designed a more polar label with increased solubility and improved membrane penetrating properties. In the newly designed probe **9**, the linker should be extended by one polar oxyethylene unit, which increases considerably the conformational flexibility. Furthermore, exchange of an F-atom at the B-atom by a methoxy moiety should additionally increase the polarity. (Figure 3)

### Interaction of **9a** and **9b** with the ion channel

In 2018, the activation mechanism of the human  $K_{Ca3.1}$  channel was elucidated by solving its molecular structure by cryo-EM (PDB 6cno).<sup>[43]</sup> This structure was used to investigate, whether the designed novel BODIPY labeled senicapoc derivatives **9a**

and **9b** can interact with the channel protein and thus can be used as molecular probes to image  $K_{Ca3.1}$  channels. The molecular modelling study was performed with the Molecular Operating Environment program version 2019 (MOE).<sup>[44]</sup>

The modelling study of compounds **9a** and **9b** led to binding modes, which are comparable to binding modes already described in previous studies.<sup>[41,42]</sup> Both compounds bind in the channel pore. However, they can only interact with their binding sites in the open state of the ion channel. (Figure 4) The senicapoc targeting unit binds at the top of the inner pore of the ion channel, whereas the linker and the connected BODIPY dye bind in the lower part of the ion channel. The additional oxyethylene moiety of **9** compared to **8** seems not to influence the interactions of **9** with  $K_{Ca3.1}$ . Moreover, replacement of one F-atom at the B-atom by a methoxy moiety was also well tolerated by the ion channel, although it changes the electronic situation within the BODIPY fluorophore considerably.

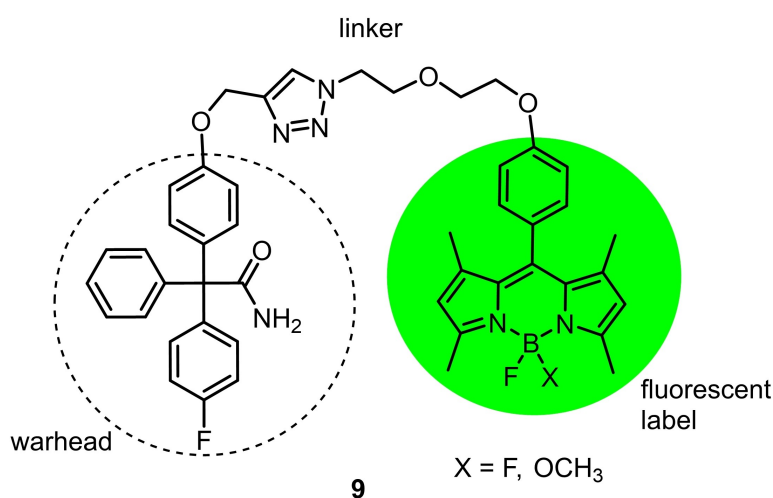


**Figure 3.** Design of novel fluorescent dye labelled senicapoc derivatives **9**. In order to increase the polarity, the linker will be extended by one oxyethylene unit and one F-atom at the B-atom will be replaced by a methoxy moiety.

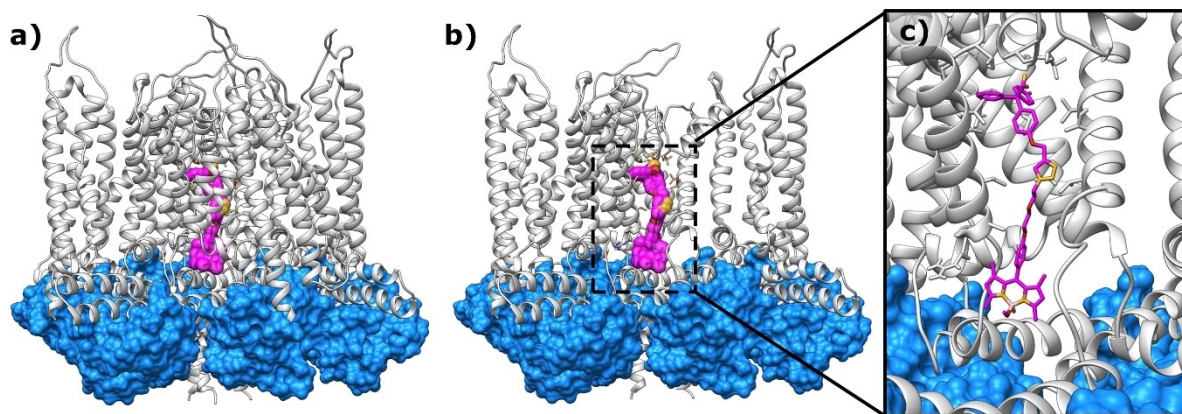


**Figure 4.** Binding of compound **9b** (magenta surface) in  $K_{Ca}3.1$  (PDB 6cno,<sup>[43]</sup> light grey:  $K_{Ca}3.1$  channel as ribbons, blue: calmodulin as surface representation). a) Compound **9b** binding in the full homotetrameric  $K_{Ca}3.1$  channel. b) **9b** bound to the channel, with one monomer removed. c) A detailed view on **9b** in the channel pore. The figures were created using UCSF Chimera.<sup>[45]</sup>

## Synthesis

The synthesis of the BODIPY dye **14a** followed a standard procedure.<sup>[46,47]</sup> According to this procedure, benzaldehyde **10** equipped with the appropriate side chain reacted with two equivalents of 2,4-dimethylpyrrole **11** in presence of  $F_3CCO_2H$  to afford the triarylmethane derivative **12**. Without isolation, **12** was oxidized with DDQ and subsequently reacted with  $BF_3 \cdot OEt_2$  to provide the BODIPY dye **14a**. The methoxy analog **14b** was obtained by activation of **14a** with TMSOTf and subsequent replacement of one F-atom with methanol.<sup>[47]</sup> In the last step a Cu-mediated 1,3-dipolar cycloaddition of the alkyne **6** with the azides **14a** and **14b** led to the desired fluorescently labeled senicapoc derivatives **9a** and **9b**. (Scheme 2)

## Lipophilicity

The conversion of the difluoro BODIPY dye **14a** into the methoxy-fluoro analog **14b** was controlled by thin layer chromatography. The exchange of one F-atom for the methoxy moiety led to a dramatic decrease of the  $R_f$  value from 0.87 (**14a**) to 0.32 (**14b**). (see Figure S1 in the Supporting Information) The decreased  $R_f$  value of **14b** correlates with increased polarity, since the  $R_f$  value reflects predominantly the interactions of a sample with polar OH moieties of silica.

The lipophilicity of the BODIPY dyes **14** and the final conjugates **9** was recorded using the recently developed micro shake flask method. After distribution between *n*-octanol and MOPS buffer pH 7.4 layers, the amount of compound in the aqueous layer was determined by mass spectrometry.<sup>[48,49]</sup> The lipophilicity of the dyes **14a** and **14b** is rather high with  $\log D_{7.4}$  values of 4.29 and 4.41, respectively. (Table 1) The increased polarity of **14b** observed during thin layer chromatography was not confirmed by its  $\log D_{7.4}$  value.  $\log D_{7.4}$  values in the range 4–5 bring the micro shake flask method to its limit, since the remaining concentration of the sample in the aqueous layer is rather low. Nevertheless, the increased lipophilicity resulting

**Table 1.**  $\log D_{7.4}$  values of the fluorescent probes **9** and the fluorescent dyes **14**.

Compd	R	$\log D_{7.4}$
<b>9a</b>	F	$4.73 \pm 0.03$
<b>9b</b>	$OCH_3$	$4.60 \pm 0.23$
<b>14a</b>	F	$4.29 \pm 0.19$
<b>14b</b>	$OCH_3$	$4.41 \pm 0.04$

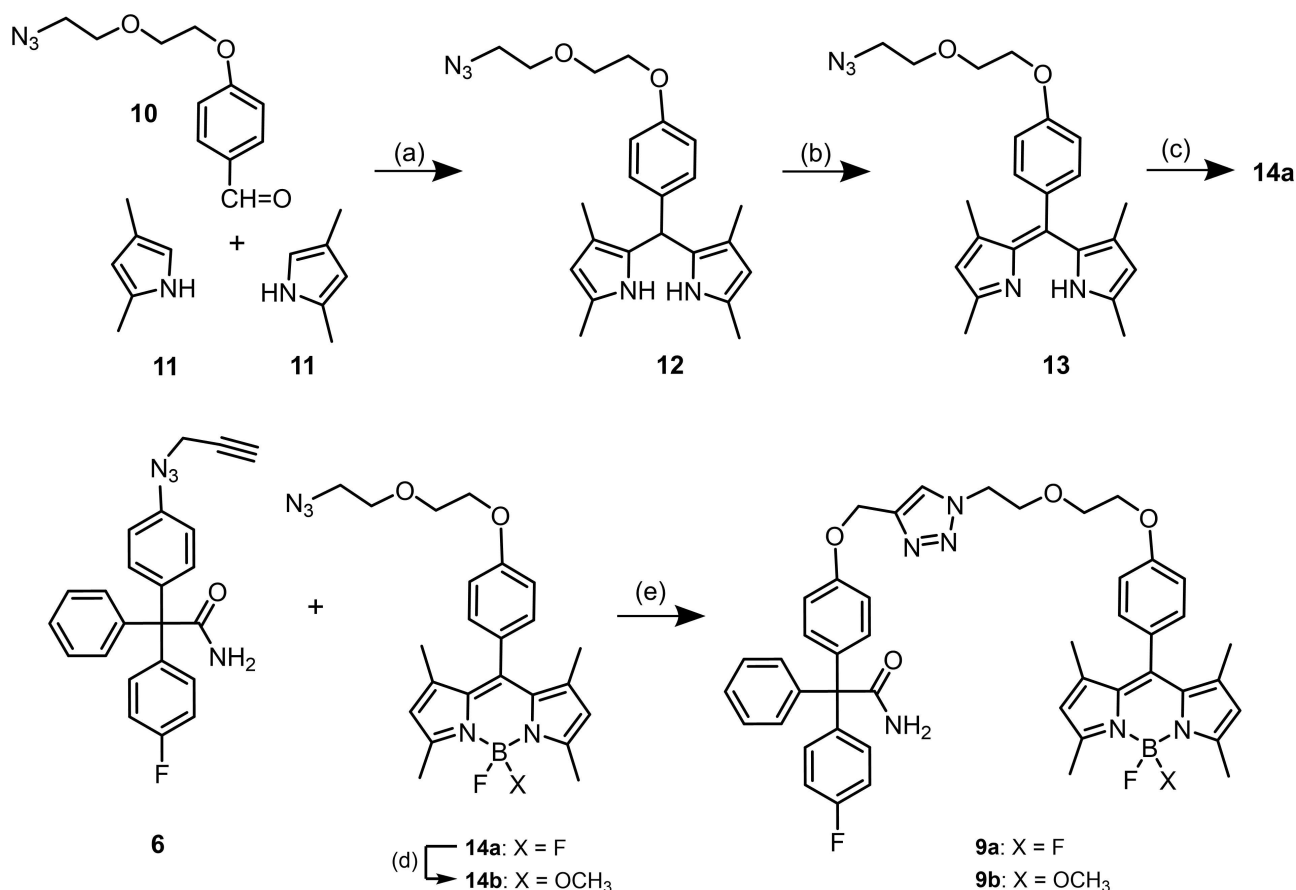
from coupling the dyes **14** with the lipophilic senicapoc targeting unit **6** to yield fluorescent probes **9** could be confirmed by the  $\log D_{7.4}$  values. However, differences between the difluoro derivatives **9a/14a** and the methoxy-fluoro derivatives **9b/14b** are not significant. Compared to **8** ( $\log D_{7.4} = 2.86 \pm 0.15$ ), the recorded  $\log D_{7.4}$  value of **9a** with a longer linker between the BODIPY dye and the triazole moiety is unexpectedly higher ( $\log D_{7.4}(\mathbf{9a}) = 4.73 \pm 0.03$ ).

## Photophysical properties

Since staining of  $K_{Ca}3.1$  channels should be analyzed by fluorescence microscopy, photophysical properties of the senicapoc BODIPY conjugates **9a** and **9b** are of high interest. Since the senicapoc targeting unit and the BODIPY itself are not in direct conjugation with each other in **9**, the precursor azides **14a** and **14b** were photophysically characterized instead of the final products. Table 2 shows both the absorption and emission maxima ( $\lambda_{max}$ ) as well as the Stokes shift, photoluminescence lifetimes ( $\tau$ ) and absolute quantum yields ( $\Phi_F$ ).

Due to their structural analogy, the difluoro derivative **14a** and the methoxy-fluoro derivative **14b** have comparable photophysical properties. The obtained absorption and emission maxima, as well as the Stokes shift of roughly 15 nm, match perfectly to commercially available filter sets for fluorescence microscopy. As shown in Table 2, the photoluminescence lifetime  $\tau$  of the methoxy-fluoro derivative **14b** is slightly shorter than for the difluoro derivative **14a**. In addition, both molecules





**Scheme 2.** Synthesis of senicapoc BODIPY conjugates. Reagents and reaction conditions: (a) F<sub>3</sub>CCO<sub>2</sub>H, CH<sub>2</sub>Cl<sub>2</sub>, rt, 24 h. (b) DDQ, CH<sub>2</sub>Cl<sub>2</sub>, rt, 30 min. (c) BF<sub>3</sub>·OEt<sub>2</sub>, NEt<sub>3</sub>, rt, 16 h, 13% (over three steps). (d) TMSOTf, CH<sub>2</sub>Cl<sub>2</sub>, 0°C, 2.5 min; then CH<sub>3</sub>OH, DIPEA, 0°C, 5 min, 39%. (e) CuSO<sub>4</sub>, Na-ascorbate, DMF, H<sub>2</sub>O, rt, 16 h, 43% (**9a**), 25% (**9b**). Details for the synthesis of aldehyde **10** are given in the Supporting Information.

**Table 2.** Photophysical properties of fluorescent dyes **14a** and **14b**.<sup>[a]</sup>

Compd	R	absorption $\lambda_{\text{max}}$ [nm]	emission $\lambda_{\text{max}}$ [nm]	Stokes shift [nm]	$\tau$ [ns]	$\Phi_F \pm 0.02$
<b>14a</b>	F	501	515	14	$3.80 \pm 0.02$	0.48
<b>14b</b>	OCH <sub>3</sub>	501	516	15	$3.50 \pm 0.01$	0.43

[a] Data were recorded in solution (CH<sub>2</sub>Cl<sub>2</sub>,  $c = 10^{-5}$  M) at 298 K. In both cases, the emission was monitored by exciting at  $\lambda_{\text{ex}} = 350$  nm (photoluminescence spectra) and  $\lambda_{\text{ex}} = 376$  nm ( $\tau$ ). Absorption and emission spectra can be seen in the Supporting Information, Figures S2 and S3; raw time-resolved photoluminescence decays are available in the SI, Figures S4 and S5.

exhibited comparably efficient quantum yields ( $\Phi_F$  values). The difluoro BODIPY **14a** shows a quantum yield of 48%, whereas  $\Phi_F$  of the methoxy-fluoro analog **14b** is slightly reduced to 43%. Aside from this slight difference (due to the uncertainty of the method, both values are almost equivalent), the two molecules have sufficiently high quantum yields  $\Phi_F$  and prominent absorption maxima to be used as bright labels in fluorescence microscopy.

#### In vitro imaging of non-small cell lung cancer cells A549-3R

We used the non-small cell lung cancer (NSCLC) cell line A549-3R overexpressing the K<sub>Ca</sub>3.1 channel for the staining

experiments.<sup>[50]</sup> The imaging properties of the new fluorescent probes were analyzed with an optimized staining protocol. According to this protocol, the fluorescent probes **9a** and **9b** were dissolved in PBS (10  $\mu$ M) and 100  $\mu$ L of the staining solution were added to a glass bottom dish, containing the adherent A549-3R tumor cells. The complete set-up was incubated for 20 min at room temperature in a dark chamber and the dish was washed 5 times with PBS afterwards. We used an Axiovert 200 microscope with a  $\times 100$  1.45 oil immersion objective connected to a RT-SE-Spot camera (Visitron, Puchheim, Germany). Image acquisition was controlled by MetaVue software.

Incubation of A549-3R cells with both probes **9a** and **9b** for 20 min resulted in the typical punctate staining pattern of the

K<sub>Ca</sub>3.1 channel in the cell membrane. (Figure 5A–D). The size of the single dots was analyzed in detail after staining the A549-3R cells with compounds **9a** and **9b** according to staining protocol 1. For this purpose, squares of 50×50 pixels were defined and the dots within the squares were analyzed. It has been shown

that a single channel has a Full Width at Half Maximum (FWHM) of  $\leq 5$  pixels corresponding to  $\approx 300$  nm.<sup>[41,42]</sup> According to our measurements, the dots for the difluoro derivative **9a** (FWHM:  $7.75 \pm 0.70$  pixel, N=3) were larger than 5 pixels. On the other side, the dots for compound **9b** bearing a methoxy group and a

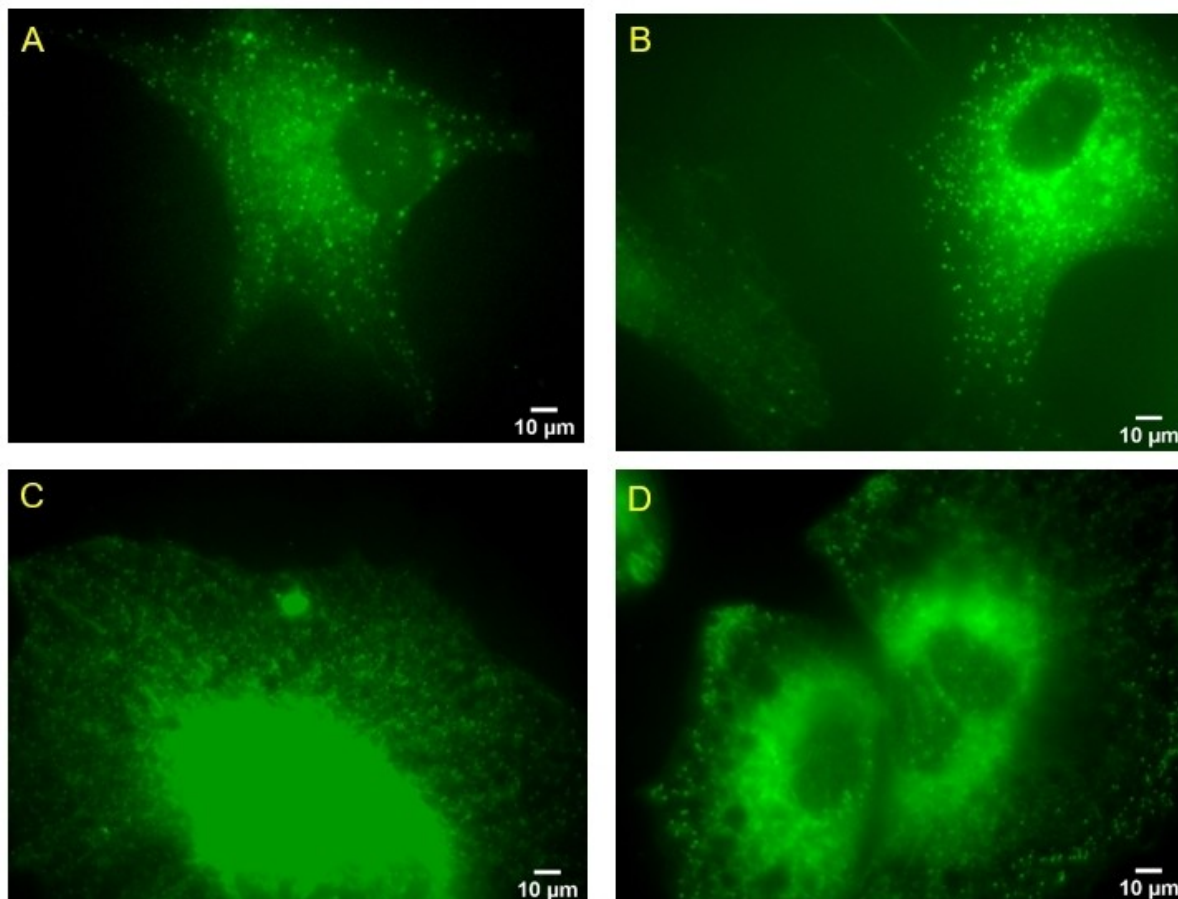


**Figure 5.** Staining of NSCLC tumor cells A549-3R with senicapoc BODIPY conjugates. 5 A,B; Staining with difluoro derivative **9a**; 5 C,D: Staining with methoxy-fluoro derivative **9b**.

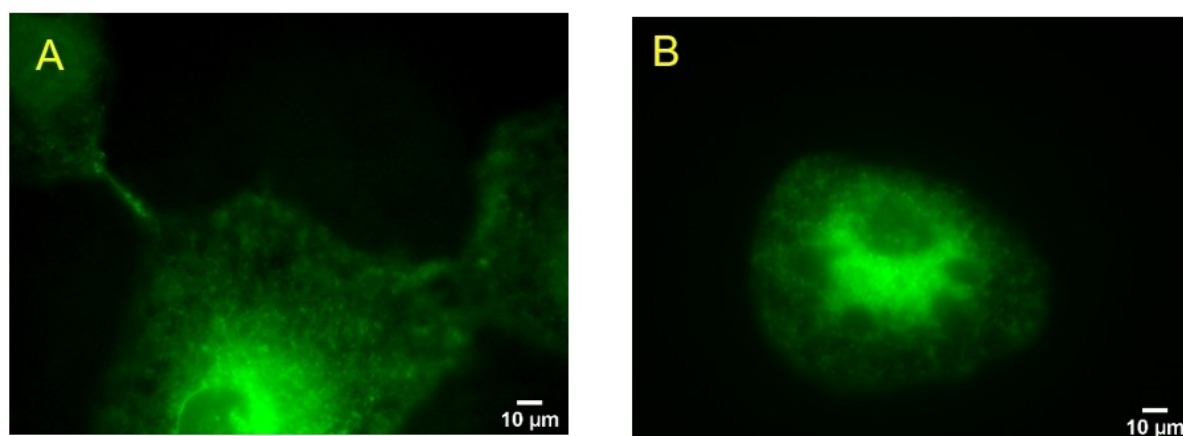


**Figure 6.** Staining of NSCLC tumor cells A549-3R after preincubation with senicapoc. A549-3R cells were preincubated with senicapoc (30 μM, 100 μL) and incubated with **9a** (Figure 6A) and **9b** (Figure 6B). The staining solutions contained senicapoc (100 μL) as well.

F-atom at the B-atom displayed a size in the range of 5 pixels (FWHM:  $5.04 \pm 0.44$  pixel,  $N=3$ ) indicating single  $K_{Ca3.1}$  channel staining.

We concluded that the more polar methoxy-fluoro derivative **9b** is superior to the difluoro derivative **9a** with respect to precise  $K_{Ca3.1}$  channel labeling. The same punctate staining pattern was observed for the first generation of probes, containing a shorter linker with only one oxyethylene moiety.<sup>[41,42]</sup>

In order to test, whether the senicapoc BODIPY conjugates **9** label selectively the  $K_{Ca3.1}$  channel, blocking experiments were performed. In these experiments, A549-3R cells were preincubated with an excess of senicapoc to occupy all binding sites in the channel pore. Subsequently, the cells were treated with staining solutions containing **9a** or **9b** (10  $\mu$ M). After preincubation with senicapoc, the previously observed punctate staining of the single  $K_{Ca3.1}$  channels was no longer detected. (Figure 6) We concluded that the senicapoc BODIPY conjugates **9a** and **9b** compete with senicapoc for its binding site at the  $K_{Ca3.1}$  channel.

## Conclusion

The 18-F-labeled PET tracer [ $^{18}$ F]**7** with a fluoroethyltriazolyl moiety represents a promising molecular probe to image  $K_{Ca3.1}$  ion channels *in vivo* (mouse). The senicapoc BODIPY conjugate **9b** is able to label selectively single  $K_{Ca3.1}$  channels in A549-3R NSCLC tumor cells. To our delight, the fluorescence quantum yield of **9b** is only marginally reduced, while the methoxy moiety at the B-atom and the additional oxyethylene unit in the spacer increase the polarity and thus improve the solubility and the general handling of **9b**. Preincubation with an excess of senicapoc led to removal of the punctate staining pattern confirming the high specificity of **9b** to interact with  $K_{Ca3.1}$  channels.

## Experimental Section

### Chemistry, general

Oxygen and moisture sensitive reactions were carried out under nitrogen, dried with silica gel with moisture indicator (orange gel, VWR, Darmstadt, Germany) and in dry glassware (Schlenk flask or Schlenk tube). All solvents were of analytical or technical grade quality. Thin layer chromatography (tlc): tlc silica gel 60  $F_{254}$  on aluminum sheets (VWR). Flash chromatography (fc): Silica gel 60, 40–63  $\mu$ m (VWR); parentheses include: diameter of the column ( $\varnothing$ ), length of the stationary phase (l), fraction size (v) and eluent. Automated flash chromatography: Isolera<sup>TM</sup> Spektra One (Biotage<sup>®</sup>); parentheses include: cartridge size, flow rate, eluent, fractions size was always 20 mL. Melting point: Melting point system MP50 (Mettler Toledo, Gießen, Germany), open capillary, uncorrected. MS: MicroTOFQII mass spectrometer (Bruker Daltonics, Bremen, Germany); deviations of the found exact masses from the calculated exact masses were 5 ppm or less; the data were analyzed with DataAnalysis<sup>®</sup> (Bruker Daltonics). NMR: NMR spectra were recorded in deuterated solvents on Agilent DD2 400 MHz and 600 MHz spectrometers (Agilent, Santa Clara CA, USA); chemical shifts ( $\delta$ ) are

reported in parts per million (ppm) against the reference substance tetramethylsilane and calculated using the solvent residual peak of the undeuterated solvent; coupling constants are given with 0.5 Hz resolution; assignment of  $^1$ H and  $^{13}$ C NMR signals was supported by 2-D NMR techniques where necessary. IR: FT/IR IR Affinity<sup>®</sup>-1 spectrometer (Shimadzu, Düsseldorf, Germany) using ATR technique.

### HPLC methods for the determination of the purity

#### HPLC method 1

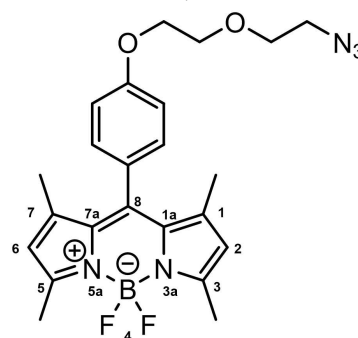
HPLC: Merck Hitachi Equipment; UV detector: L-7400; autosampler: L-7200; pump: L-7100; degasser: L-7614; column: LiChrospher<sup>®</sup> 60 RP-select B (5  $\mu$ m); LiChroCART-250–4 mm cartridge; flow rate: 1.0 mL/min; injection volume: 5.0 or 10  $\mu$ L; detection at  $\lambda=210$  nm; solvents: A: water with 0.05% (v/v) trifluoroacetic acid; B: acetonitrile with 0.05% (v/v) trifluoroacetic acid; gradient elution: (A %): 0–4 min: 90%, 4–29 min: 90→0%, 29–31 min: 0%, 31–31.5 min: 0→90%, 31.5–40 min: 90%. Data acquisition: HSM software; manual integration.

#### HPLC method 2

An Ultimate system by Thermo Scientific was used to determine the purity of the synthesized compounds at a detection wavelength of 210 nm: guard column: Zorbax SB–Aq 12.5×4.6 mm cartridge; column: Zorbax SB–Aq StableBond analytical 150×4.6 mm; UV-detector: UltiMate VWD-3400RS variable Wavelength Detector; autosampler: UltiMate 3000; pump: Ultimate LPG-3400SD; degasser: Ultimate AFC-3000; data acquisition: Chromeleon Client 6.80 (Dionex Corpor). Data were evaluated by manual integration. Gradient used to determine purities via HPLC, Tetrabutylammonium phosphate buffer (5 mM) in  $H_2O/CH_3CN$ , flow rate: 1.0 mL min<sup>−1</sup> at room temperature; 0 min: 20%  $CH_3CN$ , 20 min: 80%  $CH_3CN$ , 30 min: 20%  $CH_3CN$ .

### Synthetic procedures

#### 8-[4-(2-(2-Azidoethoxy)ethoxy)phenyl]-4,4-difluoro-1,3,5,7-tetramethyl-4-bora-3a,4a-diaza-s-indacene (**14a**)

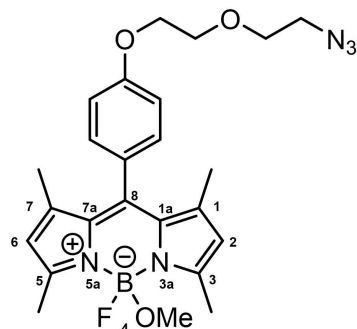


Under moisture, oxygen, and light free conditions, 2,4-dimethylpyrrole (**11**, 0.61 mL, 5.95 mmol, 2.0 eq.) and benzaldehyde **10** (700 mg, 2.98 mmol, 1.0 eq.) were dissolved in dry  $CH_2Cl_2$  (80 mL). Trifluoroacetic acid (2 drops) was added and the mixture stirred at room temperature for 24 h (→**12**). A solution of 2,3,5,6-tetrachloro-1,4-benzoquinone (722 mg, 2.98 mmol, 1.0 eq.) in  $CH_2Cl_2$  (20 mL) was added and the mixture was stirred at room temperature for 30 min (→**13**).  $Et_3N$  (2.3 mL, 16.39 mmol, 5.5 eq.) was added and the mixture was stirred at room temperature for 15 min.  $BF_3 \cdot OEt_2$



(2.3 mL, 17.9 mmol, 6 eq.) was added slowly dropwise and the mixture was stirred at room temperature overnight (16 h). H<sub>2</sub>O (100 mL) was added to the mixture and was stirred at room temperature for 1 h. The organic layer was separated, washed with H<sub>2</sub>O (3 × 100 mL), dried (Na<sub>2</sub>SO<sub>4</sub>), filtered and concentrated *in vacuo*. The crude product was filtered over silica with CH<sub>2</sub>Cl<sub>2</sub>. The filtrate was concentrated *in vacuo* and the product was purified by automatic flash chromatography; column 1: (cartridge: SNAP KP-Sil, 50 g (Biotage®), 20% → 40% ethyl acetate in cyclohexane, 50 mL/min), column 2: (cartridge: SNAP KP-Sil, 50 g (Biotage®), 30% → 100% CH<sub>2</sub>Cl<sub>2</sub> in cyclohexane, 50 mL/min), R<sub>f</sub> = 0.42 (cyclohexane:ethyl acetate = 5:2). Orange solid, mp 138 °C, yield 170 mg (13%). Purity (HPLC, method 1): 92.8% (t<sub>R</sub> = 23.6 min). C<sub>23</sub>H<sub>26</sub>BF<sub>2</sub>N<sub>5</sub>O<sub>2</sub> (M<sub>r</sub> = 453.3). <sup>1</sup>H NMR (600 MHz, DMSO): δ (ppm) = 1.40 (s, 6H, 1-CH<sub>3</sub>, 7-CH<sub>3</sub>(indacene)), 2.44 (s, 6H, 3-CH<sub>3</sub>, 5-CH<sub>3</sub>(indacene)), 3.44 (t, J = 4.3 Hz, 2H, OCH<sub>2</sub>CH<sub>2</sub>N<sub>3</sub>), 3.69 (t, J = 4.7 Hz, 2H, OCH<sub>2</sub>CH<sub>2</sub>N<sub>3</sub>), 3.82 (t, J = 4.3 Hz, 2H, OCH<sub>2</sub>CH<sub>2</sub>O), 4.18 (t, J = 4.7 Hz, 2H, OCH<sub>2</sub>CH<sub>2</sub>O), 6.17 (s, 2H, 2-CH, 6-CH(indacene)), 7.12 (d, J = 8.7 Hz, 2H, 3-H, 5-H (Ph)), 7.26 (d, J = 8.6 Hz, 2H, 2-H, 6-H (Ph)). <sup>13</sup>C NMR (151 MHz, DMSO-d<sub>6</sub>): δ (ppm) = 14.2 (4 C, 1-CH<sub>3</sub>, 3-CH<sub>3</sub>, 5-CH<sub>3</sub>, 7-CH<sub>3</sub>(indacene)), 49.9 (1 C, OCH<sub>2</sub>CH<sub>2</sub>N<sub>3</sub>), 67.2 (1 C, OCH<sub>2</sub>CH<sub>2</sub>O), 68.8 (1 C, OCH<sub>2</sub>CH<sub>2</sub>O), 69.4 (1 C, OCH<sub>2</sub>CH<sub>2</sub>N<sub>3</sub>), 115.2 (2 C, C-3, C-5 (Ph)), 121.3 (2 C, C-2, C-6(indacene)), 126.0 (1 C, C-8(indacene)), 129.1 (2 C, C-2, C-6 (Ph)), 131.1 (2 C, C-7a, C-8a(indacene)), 142.1 (1 C, C-1 (Ph)), 142.7 (2 C, C-1, C-7(indacene)), 154.6 (2 C, C-3, C-5(indacene)), 159.1 (1 C, C-4 (Ph)). Exact mass (ESI): (m/z) = 454.2220 (calcd. 454.2238 for C<sub>23</sub>H<sub>26</sub>BF<sub>2</sub>N<sub>5</sub>O<sub>2</sub> [M + H]<sup>+</sup>). IR (neat): ν<sup>-</sup> (cm<sup>-1</sup>) = 2928 (C–H, aliph), 2870 (C–H, aliph), 2114 (N=N=N), 1546 (C=C, arom), 1508 (C=C, arom), 1408 (B–F).

**8-[4-(2-(2-Azidoethoxy)ethoxy)phenyl]-4-fluoro-4-methoxy-1,3,5,7-tetramethyl-4-bora-3,4,4a-diaza-s-indacene (14b)**

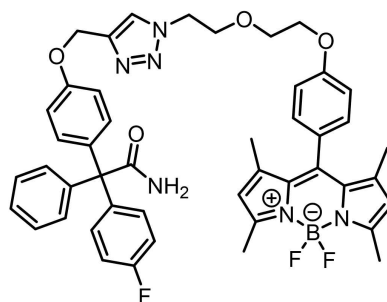


Under N<sub>2</sub>, BODIPY dye **14a** (150 mg, 0.33 mmol, 1.0 eq.) was dissolved in CH<sub>2</sub>Cl<sub>2</sub> (50 mL). The solution was cooled to 0 °C on ice and under stirring TMSOTf (0.3 mL, 1.65 mmol, 5 eq.) was added. The solution was stirred for 2.5 min. Methanol (1.34 mL, 33.1 mmol, 100 eq.) and DIPEA (0.58 mL, 3.31 mmol, 10 eq.) were injected into the solution and the solution was stirred for 5 min. H<sub>2</sub>O (50 mL) was added and the mixture was stirred for 20 min at room temperature. The organic layer was separated, washed with H<sub>2</sub>O (3 × 50 mL), dried (Na<sub>2</sub>SO<sub>4</sub>), filtered and concentrated *in vacuo*. The crude product was purified by flash column chromatography; column 1: (ø = 2.5 cm, h = 20 cm, V = 10 mL, CH<sub>2</sub>Cl<sub>2</sub>:MeOH = 98:2), column 2: (ø = 2.5 cm, h = 20 cm, V = 10 mL, toluene:acetonitrile = 4:1), R<sub>f</sub> = 0.34 (CH<sub>2</sub>Cl<sub>2</sub>:MeOH = 98:2).

Orange solid, mp 88–89 °C, yield (39%). Purity (HPLC, method 1): 95.3% (t<sub>R</sub> = 27.3 min). C<sub>24</sub>H<sub>29</sub>BF<sub>3</sub>N<sub>5</sub>O<sub>3</sub> (M<sub>r</sub> = 465.3). <sup>1</sup>H NMR (600 MHz, DMSO): δ (ppm) = 1.39 (s, 6H, 1-CH<sub>3</sub>, 7-CH<sub>3</sub>(indacene)), 2.43 (s, 6H, 3-CH<sub>3</sub>, 5-CH<sub>3</sub>(indacene)), 2.81 (s, 3H, OCH<sub>3</sub>), 3.44 (t, J = 5.6 Hz, 2H, OCH<sub>2</sub>CH<sub>2</sub>N<sub>3</sub>), 3.69 (t, J = 5.5 Hz, 2H, OCH<sub>2</sub>CH<sub>2</sub>N<sub>3</sub>), 3.79–3.84 (m, 2H, OCH<sub>2</sub>CH<sub>2</sub>O), 4.14–4.19 (m, 2H, OCH<sub>2</sub>CH<sub>2</sub>O), 6.13 (s, 2H, 2-CH, 6-CH(indacene)), 7.07–7.15 (m, 2H, 3-H, 5-H (Ph)), 7.19–7.28 (m, 2H, 2-H, 6-H (Ph)). <sup>13</sup>C NMR

(151 MHz, DMSO-d<sub>6</sub>): δ (ppm) = 14.2 (4 C, 1-CH<sub>3</sub>, 3-CH<sub>3</sub>, 5-CH<sub>3</sub>, 7-CH<sub>3</sub>(indacene)), 48.5 (1 C, OCH<sub>3</sub>), 49.9 (1 C, OCH<sub>2</sub>CH<sub>2</sub>N<sub>3</sub>), 67.2 (1 C, OCH<sub>2</sub>CH<sub>2</sub>O), 68.8 (1 C, OCH<sub>2</sub>CH<sub>2</sub>O), 69.4 (1 C, OCH<sub>2</sub>CH<sub>2</sub>N<sub>3</sub>), 115.1 (2 C, C-3, C-5 (Ph)), 121.0 (2 C, C-2, C-6(indacene)), 126.5 (1 C, C-8(indacene)), 129.2 (2 C, C-2, C-6 (Ph)), 131.9 (2 C, C-7a, C-8a(indacene)), 141.6 (1 C, C-1 (Ph)), 141.9 (2 C, C-1, C-7(indacene)), 154.6 (2 C, C-3, C-5(indacene)), 159.0 (1 C, C-4 (Ph)). Exact mass (ESI): (m/z) = 466.2361 (calcd. 466.2420 for C<sub>24</sub>H<sub>29</sub>BF<sub>3</sub>N<sub>5</sub>O<sub>3</sub> [M + H]<sup>+</sup>). IR (neat): ν<sup>-</sup> (cm<sup>-1</sup>) = 2866 (C–H, aliph), 2808 (C–H, aliph), 2110 (N=N=N), 1543 (C=C, arom), 1508 (C=C, arom), 1249 (C–O).

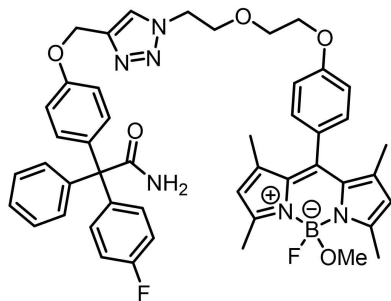
**2-{4-[(1-{2-[4-(4,4-Difluoro-1,3,5,7-tetramethyl-4-bora-3,4,4a-diaza-s-indacene-8-yl)phenoxy]ethylethoxy)-1,2,3-triazol-4-yl)methoxy]phenyl}-2-(4-fluorophenyl)-2-phenylacetamide (9a)**



BODIPY azide **14a** (26.7 mg, 0.06 mmol, 1.0 eq.) and propargyl ether **6**<sup>[41]</sup> (21.2 mg, 0.06 mmol, 1.0 eq.) were dissolved in a mixture of DMF (5 mL) and H<sub>2</sub>O (4 mL). Sodium ascorbate (77.1 mg, 0.4 mmol, 6.6 eq.) and CuSO<sub>4</sub> (61.2 mg, 0.4 mmol, 6.5 eq.) were added. The solution was stirred at room temperature for 16 h. LiCl solution (5% wt in H<sub>2</sub>O, 10 mL) was added. The organic layer was separated and washed with LiCl solution (5% wt in H<sub>2</sub>O, 3 × 10 mL). The organic layer was dried (Na<sub>2</sub>SO<sub>4</sub>), filtered and concentrated *in vacuo*. The crude product was purified by flash column chromatography (ø = 2.5 cm, h = 15 cm, V = 2 mL, CH<sub>2</sub>Cl<sub>2</sub>:MeOH = 95:5), automatic flash chromatography 1: (cartridge: SNAP KP-Sil, 10 g (Biotage®), 50% → 85% ethyl acetate in cyclohexane, 12 mL/min), automatic flash chromatography 2: (cartridge: SNAP C18, 12 g (Biotage®), 60% → 100% CH<sub>3</sub>CN in water, 12 mL/min), R<sub>f</sub> = 0.34 (cyclohexane:ethyl acetate = 1:5). Orange solid, mp 103 °C, yield 21 mg (43%). Purity (HPLC, method 2): 91.6% (t<sub>R</sub> = 20.9 min). C<sub>46</sub>H<sub>44</sub>BF<sub>3</sub>N<sub>6</sub>O<sub>4</sub> (M<sub>r</sub> = 812.7). <sup>1</sup>H NMR (600 MHz, DMSO-d<sub>6</sub>): δ (ppm) = 1.38 (s, 6H, 1-CH<sub>3</sub>, 7-CH<sub>3</sub>(indacene)), 2.44 (s, 6H, 3-CH<sub>3</sub>, 5-CH<sub>3</sub>(indacene)), 3.74–3.82 (m, 2H, OCH<sub>2</sub>CH<sub>2</sub>N), 3.91 (t, J = 5.2 Hz, 2H, OCH<sub>2</sub>CH<sub>2</sub>O), 4.09–4.15 (m, 2H, OCH<sub>2</sub>CH<sub>2</sub>N), 4.59 (t, J = 5.2 Hz, 2H, OCH<sub>2</sub>CH<sub>2</sub>O), 5.11 (s, 2H, aryl-CH<sub>2</sub>O), 6.15 (s, 2H, 2-CH, 6-CH(indacene)), 6.61 (bs, 1H, NH<sub>2</sub>), 6.96 (d, J = 9.0 Hz, 2H, 2-H, 6-H (OPh)), 7.06–7.12 (m, 6H, 3-H, 5-H (OPh), 3-H, 5-H (FPh), 3-H, 5-H (dye-Ph)), 7.14–7.25 (m, 7H, 2-H, 6-H (dye-Ph), 2-H, 6-H (Ph), 2-H, 6-H (FPh), 4-H (Ph)), 7.25–7.31 (m, 2H, 3-H, 5-H (Ph)), 7.52 (bs, 1H, NH<sub>2</sub>), 8.23 (s, 1H, CH(triazole)). <sup>13</sup>C NMR (151 MHz, DMSO-d<sub>6</sub>): δ (ppm) = 14.2 (4 C, 1-CH<sub>3</sub>, 3-CH<sub>3</sub>, 5-CH<sub>3</sub>, 7-CH<sub>3</sub>(indacene)), 49.3 (1 C, OCH<sub>2</sub>CH<sub>2</sub>O), 61.1 (1 C, aryl-CH<sub>2</sub>O), 65.9 (1 C, CCONH<sub>2</sub>), 67.0 (1 C, OCH<sub>2</sub>CH<sub>2</sub>N), 68.6 (1 C, OCH<sub>2</sub>CH<sub>2</sub>N), 68.8 (1 C, OCH<sub>2</sub>CH<sub>2</sub>O), 113.8 (2 C, C-2, C-6 (OPh)), 114.2 (d, J = 21.0 Hz, 2 C, C-3, C-5 (FPh)), 115.2 (2 C, C-3, C-5 (dye-Ph)), 121.2 (2 C, C-2, C-6(indacene)), 124.9 (1 C, C-5(triazole)), 126.0 (1 C, C-4 (Ph)), 126.5 (1 C, C-8(indacene)), 129.1 (2 C, C-2, C-6(dye-Ph)), 129.9 (2 C, C-2, C-6 (Ph)), 131.1 (2 C, C-7a, C-8a(indacene)), 131.2 (2 C, C-3, C-5 (OPh)), 132.0 (d, J = 8.0 Hz, 2 C, C-2, C-6 (FPh)), 136.0 (1 C, C-4 (OPh)), 140.4 (d, J = 3.0 Hz, 1 C, C-1 (FPh)), 142.1 (1 C, C-1 (Ph)), 142.5 (2 C, C-1, C-7(indacene)), 142.7 (1 C, C-4(triazole)), 144.0 (1 C, C-1 (OPh)), 154.6 (2 C, C-3, C-5(indacene)), 156.5 (1 C, C-1 (OPh)), 159.0 (1 C, C-4 (dye-Ph)), 160.6 (d, J = 243.5 Hz, 1 C, C-4 (FPh)), 174.2 (1 C, CONH<sub>2</sub>). Exact mass (APCI): (m/z) = 793.3464 (calcd. 793.3480 for C<sub>46</sub>H<sub>44</sub>BF<sub>3</sub>N<sub>6</sub>O<sub>4</sub> [M–F]<sup>+</sup>). IR (neat): ν<sup>-</sup> (cm<sup>-1</sup>) = 3486 (CON–H), 2924

(C–H, aliph), 1678 (C=O), 1605 (C=C), 1543 (C=C, arom), 1504 (C=C, arom), 1470 (B–F).

2-{4-[(1-{2-[4-(4-Fluoro-4-methoxy-1,3,5,7-tetramethyl-4-bora-3,4,4a-diaza-s-indacen-8-yl)phenoxy]ethylethoxy}-1,2,3-triazol-4-yl)methoxy]phenyl}-2-(4-fluorophenyl)-2-phenylacetamide (9b)



BODIPY azide **14b** (32.2 mg, 0.07 mmol, 1.0 eq.) and propargyl ether **6** (24.9 mg, 0.07 mmol, 1.0 eq.) were dissolved in a mixture of DMF (5 mL) and H<sub>2</sub>O (4 mL). Sodium ascorbate (90.2 mg, 0.5 mmol, 6.6 eq.) and CuSO<sub>4</sub> (71.6 mg, 0.5 mmol, 6.5 eq.) were added. The solution was stirred at room temperature for 16 h. LiCl solution (5 % wt in H<sub>2</sub>O, 10 mL) were added. The organic layer was separated and washed with LiCl solution (5 % wt in H<sub>2</sub>O, 3 × 10 mL). The organic layer was dried (Na<sub>2</sub>SO<sub>4</sub>), filtered and concentrated *in vacuo*. The crude product was purified by automatic flash chromatography 1: (cartridge: SNAP KP-Sil, 10 g (Biotage®), 60 % → 85 % ethyl acetate in cyclohexane, 12 mL/min), automatic flash chromatography 2: (cartridge: SNAP C18, 12 g (Biotage®), 30 % → 100 % CH<sub>3</sub>CN in water, 12 mL/min), R<sub>f</sub> = 0.32 (cyclohexane:ethyl acetate = 1:4). Orange solid, mp 97–98 °C, yield 14 mg (25 %). Purity (HPLC, method 2): 93.6 % (t<sub>R</sub> = 21.2 min). C<sub>47</sub>H<sub>47</sub>BF<sub>2</sub>N<sub>6</sub>O<sub>5</sub> (M<sub>r</sub> = 824.7). <sup>1</sup>H NMR (600 MHz, DMSO-*d*<sub>6</sub>): δ (ppm) = 1.37 (s, 6H, 1-CH<sub>3</sub>, 7-CH<sub>3</sub>(indacene)), 2.42 (s, 6H, 3-CH<sub>3</sub>, 5-CH<sub>3</sub>(indacene)), 2.79 (s, 3H, OCH<sub>3</sub>), 3.72–3.82 (m, 2H, OCH<sub>2</sub>CH<sub>2</sub>N), 3.91 (t, *J* = 5.2 Hz, 2H, OCH<sub>2</sub>CH<sub>2</sub>O), 4.10–4.13 (m, 2H, OCH<sub>2</sub>CH<sub>2</sub>N), 4.59 (t, *J* = 5.2 Hz, 2H, OCH<sub>2</sub>CH<sub>2</sub>O), 5.11 (s, 2H, aryl-CH<sub>2</sub>O), 6.11 (s, 2H, 2-CH, 6-CH(indacene)), 6.62 (bs, 1H, NH<sub>2</sub>), 6.96 (d, *J* = 9.0 Hz, 2H, 2-H, 6-H<sub>(OPh)</sub>), 7.04–7.12 (m, 6H, 3-H, 5-H<sub>(OPh)</sub>, 3-H, 5-H<sub>(FPh)</sub>, 3-H, 5-H<sub>(dye-Ph)</sub>), 7.13–7.24 (m, 7H, 2-H, 6-H<sub>(dye-Ph)</sub>, 2-H, 6-H<sub>(Ph)</sub>, 2-H, 6-H<sub>(FPh)</sub>, 4-H<sub>(Ph)</sub>), 7.25–7.34 (m, 2H, 3-H, 5-H<sub>(Ph)</sub>), 7.52 (bs, 1H, NH<sub>2</sub>), 8.23 (s, 1H, CH<sub>(triazole)</sub>). <sup>13</sup>C NMR (151 MHz, DMSO-*d*<sub>6</sub>): δ (ppm) = 14.0–14.3 (4 C, 1-CH<sub>3</sub>, 3-CH<sub>3</sub>, 5-CH<sub>3</sub>, 7-CH<sub>3</sub>(indacene)), 48.4 (d, *J* = 6.5 Hz, 1 C, OCH<sub>3</sub>), 49.3 (1 C, OCH<sub>2</sub>CH<sub>2</sub>O), 61.1 (1 C, aryl-CH<sub>2</sub>O), 65.9 (1 C, CCONH<sub>2</sub>), 67.0 (1 C, OCH<sub>2</sub>CH<sub>2</sub>N), 68.6 (1 C, OCH<sub>2</sub>CH<sub>2</sub>N), 68.8 (C1, OCH<sub>2</sub>CH<sub>2</sub>O), 113.8 (2 C, C-2, C-6<sub>(OPh)</sub>), 114.2 (d, *J* = 21.2 Hz, 2 C, C-3, C-5<sub>(FPh)</sub>), 115.1 (d, *J* = 11.0 Hz, 2 C, C-3, C-5<sub>(dye-Ph)</sub>), 121.0 (2 C, C-2, C-6<sub>(indacene)</sub>), 124.9 (1 C, C-5<sub>(triazole)</sub>), 126.5 (d, *J* = 3.9 Hz, 1 C, C-8<sub>(indacene)</sub>), 127.7 (1 C, 4-C<sub>(Ph)</sub>), 129.2 (d, *J* = 2.7 Hz, 2 C, C-2, C-6<sub>(dye-Ph)</sub>), 129.9 (2 C, C-2, C-6<sub>(Ph)</sub>), 131.2 (2 C, C-3, C-5<sub>(OPh)</sub>), 131.9 (2 C, C-7a, C-8a<sub>(indacene)</sub>), 132.0 (d, *J* = 8.0 Hz, 2 C, C-2, C-6<sub>(FPh)</sub>), 136.0 (1 C, C-4<sub>(OPh)</sub>), 140.4 (d, *J* = 3.0 Hz, 1 C, C-1<sub>(FPh)</sub>), 141.6 (1 C, C-1<sub>(Ph)</sub>), 141.9 (2 C, C-1, C-7<sub>(indacene)</sub>), 142.5 (1 C, C-4<sub>(triazole)</sub>), 144.0 (1 C, C-1<sub>(Ph)</sub>), 154.6 (2 C, C-3, C-5<sub>(indacene)</sub>), 156.5 (1 C, C-1<sub>(OPh)</sub>), 158.9 (1 C, C-4<sub>(dye-Ph)</sub>), 160.6 (d, *J* = 243.8 Hz, 1 C, C-4<sub>(FPh)</sub>), 174.2 (1 C, CONH<sub>2</sub>). Exact mass (ESI): (m/z) = 793.3467 (calcd. 793.3480 for C<sub>46</sub>H<sub>44</sub>BF<sub>3</sub>N<sub>6</sub>O<sub>4</sub> [M-OMe]<sup>+</sup>). IR (neat): ν̃ (cm<sup>-1</sup>) = 3483 (CON–H), 2927 (C–H, aliph), 1678 (C=O), 1605 (C=C), 1543 (C=C, arom), 1504 (C=C, arom), 1242 (C–O).

## Materials for cell staining

10 mM stock solutions of **9a** and **9b** were prepared in a glass vial with DMSO as solvent. The staining solutions of **9a** and **9b** (10 μM) were obtained by diluting the stock solutions with phosphate

buffered saline (PBS, 1:1000) in a microcentrifuge tube (Eppendorf®) and dissolving the precipitate by using a Vortex (Scientific®) for 5 min.

## Cell culture and staining

**Cell culture.** We used the non-small lung adenocarcinoma cell line A549-3R. The suffix “3R” refers to the repeated process of intravenous administration of parental cells (also initially “0R”) into immunocompromised mice to select for tumor cells with high metastatic potential.<sup>[25,41,42]</sup> A549-3R cells overexpress K<sub>Ca</sub>3.1 channels and thus are suitable for corresponding staining experiments.<sup>[7]</sup> The cells were cultured in Dulbecco’s Modified Eagle’s Medium (DMEM) with 4.5 g/L glucose and supplemented with 10 % fetal calf serum (FCS Superior) at 37 °C and 5 % carbon dioxide (CO<sub>2</sub>) in cell culture dishes (Ø = 10 cm). For experiments, approximately 20,000 cells were seeded on glass bottom dishes coated with 0.1 % poly-L-lysine (30 min, room temperature) and washed with Dulbecco’s Phosphate Buffered Saline (PBS). DMEM (1 mL) was added to each dish and the cells were incubated overnight at 37 °C and 5 % CO<sub>2</sub> prior to the experiments.

**Staining protocols.** For each experiment, the medium was removed and the cells were washed three times with PBS and fixed with 3.5 % paraformaldehyde (PFA) in PBS for 30 min at room temperature. Then, the cells were washed three times with PBS at room temperature and kept for 10 min in PBS supplemented with 100 mmol/L glycine and washed again three times. Thereafter, staining with senicapoc BODIPY conjugates **9** was performed:

**Protocol 1:** The staining solution (100 μL) of **9a** or **9b** (10 μM in PBS) was pipetted into the glass bottom dish so that all cells were covered. The NSCLC cells were incubated in a humidified dark chamber for 20 min. After washing the cells five times with PBS, PBS (200 μL) was added to the glass bottom dish, which was used for fluorescence microscopy.

**Protocol 2 (blocking experiment):** 100 μL of a senicapoc solution (30 μM in PBS) was added to a glass bottom dish and incubated for 5 min. After washing with PBS once, 200 μL of a mixture of the staining solution containing the senicapoc BODIPY conjugate **9a** or **9b** (100 μL) and the senicapoc solution (100 μL) were added to the dish and incubated for 20 min in a dark chamber. After washing five times with PBS and adding 100 μL PBS, the glass bottom dish was used for fluorescence microscopy.

## Molecular modelling

The same workflow as already described by Brommel et al.<sup>[41]</sup> was used. The available cryo-EM structure of K<sub>Ca</sub>3.1 channel<sup>[43]</sup> was protonated at pH 7.4 and refined by adjusting and adding missing residues and loop segments. The final structure was inspected visually afterwards. Initially, a docking study of senicapoc was carried out using the docking software GOLD<sup>[51]</sup> with standard settings as described in ref.<sup>[41]</sup>. Afterwards, the BODIPY labelled derivatives **9a** and **9b** were modelled along the pore and minimized afterwards. The BODIPY is ~11.60 Å long and was designed to perfectly accommodate the length of the pore, allowing the fluorescent label to lay in the lower pore of the channel. The Amber10:EHT parameters and AM1-BCC<sup>[52]</sup> partial charges for small molecules were used with MOE in the modelling process.

## Supporting Information

The Supporting Information contains detailed information about the synthesis of benzaldehyde **10**, thin-layer chromatography, photophysical characterization, and  $^1\text{H}$  and  $^{13}\text{C}$  NMR spectra.

## Acknowledgments

This work was supported by the Research Training Group "Chemical biology of ion channels (Chembion)" funded by the Deutsche Forschungsgemeinschaft (DFG), which is gratefully acknowledged. Ilka Neumann's technical assistance is greatly acknowledged. C.A.S. gratefully thanks the Alexander von Humboldt Foundation for a postdoctoral scholarship granted to I.M., the Deutsche Forschungsgemeinschaft (CRC 1450 inSight – 431460824) and the Deutsche Forschungsgemeinschaft/Land NRW (INST 211/915-1 FUGG) for generous financial support. Open Access funding enabled and organized by Projekt DEAL.

## Conflict of Interest

The authors declare no conflict of interest.

## Data Availability Statement

The data that support the findings of this study are available from the corresponding author upon reasonable request.

**Keywords:** BODIPY · fluorescent probes ·  $\text{K}_{\text{Ca}}3.1$  channel · non-small cell lung cancer · positron emission tomography · senicapoc

- [1] C. Vergara, R. Latorre, N. Marrion, J. Adelman, *Curr. Opin. Neurobiol.* **1998**, *8*(3), 321–329.
- [2] L. Sforza, A. Megaro, M. Pessia, F. Franciolini, L. Catacuzzeno, *Curr. Neuropharmacol.* **2018**, *16*(5), 608–617.
- [3] C. M. Fanger, S. Ghanshani, N. J. Logsdon, H. Rauer, K. Kalman, J. Zhou, K. Beckingham, K. G. Chandy, M. D. Cahalan, J. Aiyyar, *J. Biol. Chem.* **1999**, *274*(9), 5746–5754.
- [4] J. Maylie, C. T. Bond, P. S. Hersen, W. S. Lee, J. P. Adelman, *J. Physiol.* **2004**, *554*(Pt 2), 255–261.
- [5] J. E. Matos, M. Sausbier, G. Beranek, U. Sausbier, P. Ruth, J. Leipziger, *Acta Physiol. (Oxf.)* **2007**, *189*(3), 251–258.
- [6] M. S. Valero, M. Ramón-Giménez, J. Lozano-Gerona, P. Delgado-Wicke, P. Calmarza, A. Oliván-Viguera, V. López, Á. L. García-Otín, S. Valero, E. Pueyo, K. L. Hamilton, H. Miura, R. Köhler, *Int. J. Mol. Sci.* **2019**, *20*(5), 1193.
- [7] M. Hayashi, J. Wang, S. E. Hede, I. Novak, *Am. J. Physiol. Cell Physiol.* **2012**, *303*(2), C151–159.
- [8] S. Ghanshani, H. Wulff, M. J. Miller, H. Rohm, A. Neben, G. A. Gutman, M. D. Cahalan, K. G. Chandy, *J. Biol. Chem.* **2000**, *275*(47), 37137–37149.
- [9] A. Schwab, A. Fabian, P. J. Hanley, C. Stock, *Physiol. Rev.* **2012**, *92*(4), 1865–1913.
- [10] S. Sugunan, S. Nampoothiri, T. Garg, R. Krishnamurthy, *CNS Neurol. Disord. Drug Targets* **2016**, *15*(10), 1299–1305.
- [11] C. Gross, *Epilepsy Curr.* **2020**, *20*, 211–213.
- [12] L. Jin, J. di Lucente, H. M. Nguyen, V. Singh, L. Singh, M. Chavez, T. Bushong, H. Wulff, I. Maezawa, *Ann. Clin. Transl. Neurol.* **2019**, *6*, 723–738.
- [13] I. Maezawa, D. P. Jenkins, B. E. Jin, H. Wulff, *Int. J. Alzheimers Dis.* **2012**, *2012*, 868972.
- [14] M. Yi, P. Yu, Q. Lu, H. M. Geller, Z. Yu, H. Chen, *Mol. Cell. Neurosci.* **2016**, *76*, 21–32.
- [15] I. Grgic, E. Kiss, B. P. Kaistha, C. Busch, M. Kloss, J. Sautter, A. Müller, A. Kaistha, C. Schmidt, G. Raman, H. Wulff, F. Strutz, H. J. Gröne, R. Köhler, J. Hoyer, *Proc. Natl. Acad. Sci. USA* **2009**, *106*, 14518–14523.
- [16] C. Huang, S. Shen, Q. Ma, J. Chen, A. Gill, C. A. Pollock, X. M. Chen, *Diabetes* **2013**, *62*, 2923–2934.
- [17] R. Xu, C. Li, Y. Wu, L. Shen, J. Ma, J. Qian, J. Ge, *Arterioscler. Thromb. Vasc. Biol.* **2017**, *37*, 226–236.
- [18] C. C. Chou, C. A. Lunnon, N. J. Murgolo, *Expert Rev. Mol. Diagn.* **2008**, *8*(2), 179–187.
- [19] Y. R. Zhu, X. X. Jiang, D. M. Zhang, *J. Mol. Med.* **2019**, *97*, 1219–1229.
- [20] R. Köhler, H. Wulff, I. Eichler, M. Kneifel, D. Neumann, A. Knorr, I. Grgic, D. Kämpfe, H. Si, J. Wibawa, R. Real, K. Borner, S. Brakemeier, H. D. Orzechowski, H. P. Reusch, M. Paul, K. G. Chandy, J. Hoyer, *Circulation* **2003**, *108*(9), 1119–1125.
- [21] M. Rabjerg, A. Oliván-Viguera, L. K. Hansen, L. Jensen, L. Sevelsted-Møller, S. Walter, B. L. Jensen, N. Marcussen, R. Köhler, *PLoS One* **2015**, *10*(4), e0122992.
- [22] J. Wen, B. Lin, L. Lin, Y. Chen, O. Wang, *Aging* **2020**, *12*(16), 16437–16456.
- [23] S. Ohya, K. Kimura, S. Niwa, A. Ohno, Y. Kojima, S. Sasaki, K. Kohri, Y. Imaizumi, *J. Pharmacol. Sci.* **2009**, *109*(1), 148–151.
- [24] A. Biasiotta, D. D'Arcangelo, F. Passarelli, E. M. Nicodemi, A. Facchiano, *J. Transl. Med.* **2016**, *14*, 285, 1–15.
- [25] E. Bulk, A. S. Ay, M. Hammadi, H. Ouadid-Ahidouch, S. Schelhaas, A. Hascher, C. Rohde, N. H. Thoenissen, R. Wiewrodt, E. Schmidt, A. Marra, L. Hillejan, A. H. Jacobs, H. U. Klein, M. Dugas, W. E. Berdel, C. Müller-Tidow, A. Schwab, *Int. J. Cancer* **2015**, *137*(6), 1306–1317.
- [26] M. Faouzi, F. Hague, D. Geerts, A. S. Ay, M. Potier-Cartreau, A. Ahidouch, H. Ouadid-Ahidouch, *Oncotarget* **2016**, *7*(24), 36419–36435.
- [27] N. Prevarskaya, R. Skryma, Y. Shuba, *Physiol. Rev.* **2018**, *98*, 559–621.
- [28] C. J. Mohr, F. A. Steudel, D. Gross, P. Ruth, W. Y. Lo, R. Hoppe, W. Schroth, H. Brauch, S. M. Huber, R. Lukowski, *Cancers* **2019**, *11*(109), 1–22.
- [29] Z. Pethö, K. Najder, E. Bulk, A. Schwab, *Cell Calcium* **2019**, *80*, 79–90.
- [30] C. J. Mohr, D. Gross, E. C. Sezgin, F. A. Steudel, P. Ruth, S. M. Huber, R. Lukowski, *Cancers* **2019**, *11*, 1285.
- [31] E. L. Lee, Y. Hasegawa, T. Shimizu, Y. Okada, *Am. J. Physiol. Cell Physiol.* **2008**, *294*(6), C1398–C1406.
- [32] F. Glaser, P. Hundehege, E. Bulk, L. M. Todesca, S. Schimmelpfennig, E. Nass, T. Budde, S. G. Meuth, A. Schwab, *Sci. Rep.* **2021**, *11*(1), 18330.
- [33] H. Wulff, G. A. Gutman, M. D. Cahalan, K. G. Chandy, *J. Biol. Chem.* **2011**, *276*, 32040–32045.
- [34] K. I. Ataga, W. R. Smith, L. M. De Castro, P. Swerdlow, Y. Sauntharajah, O. Castro, E. Vichinsky, A. Kutlar, E. P. Orringer, G. C. Rigdon, W. Stocker, *Blood* **2008**, *111*(8), 3991–3997.
- [35] R. Eil, S. K. Vodnala, D. Clever, C. A. Klebanoff, M. Sukumar, J. H. Pan, D. C. Palmer, A. Gros, T. N. Yamamoto, S. J. Patel, G. C. Guittard, Z. Yu, V. Carbonaro, K. Okkenhaug, D. S. Schrupp, W. M. Linehan, R. Roychoudhuri, N. P. Restifo, *Nature* **2016**, *537*(7621), 539–543.
- [36] K. G. Chandy, R. S. Norton, *Nature* **2016**, *537*(7621), 497–499.
- [37] L. M. Todesca, S. Maskri, K. Brömmel, I. Thale, B. Wünsch, O. Koch, A. Schwab, *Cell. Physiol. Biochem.* **2021**, *55*(S3), 131–144.
- [38] J. W. Stocker, L. de Franceschi, G. A. McNaughton-Smith, R. Corrocher, Y. Beuzard, C. Brugnara, *Blood* **2003**, *101*, 2412–2418.
- [39] K. Brömmel, C. P. Konken, F. Börgel, H. Obeng-Darko, S. Schelhaas, E. Bulk, T. Budde, A. Schwab, M. Schäfers, B. Wünsch, *RSC Adv.* **2021**, *11*, 30295–30304.
- [40] C. P. Konken, K. Heßling, I. Thale, S. Schelhaas, J. Dabel, S. Maskri, E. Bulk, T. Budde, O. Koch, A. Schwab, M. Schäfers, B. Wünsch, *Arch. Pharm.* **2022**, e2200388.
- [41] K. Brömmel, S. Maskri, I. Maisuls, C. P. Konken, M. Rieke, Z. Pethö, C. A. Strassert, O. Koch, A. Schwab, B. Wünsch, *Angew. Chem. Int. Ed.* **2020**, *59*, 8277–8284; *Angew. Chem.* **2020**, *132*, 8354–8361.
- [42] K. Brömmel, S. Maskri, E. Bulk, Z. Pethö, M. Rieke, T. Budde, O. Koch, A. Schwab, B. Wünsch, *ChemMedChem* **2020**, *15*, 2462–2469.
- [43] C. H. Lee, R. MacKinnon, *Science* **2018**, *360*(6388), 508–513.
- [44] Molecular Operating Environment (MOE) **2019**. Chemical Computing Group ULC, 1010 Sherbrooke St. West, Suite #910, Montreal, QC, Canada, H3A 2R7.
- [45] E. F. Pettersen, T. D. Goddard, C. C. Huang, G. S. Couch, D. M. Greenblatt, E. C. Meng, T. E. Ferrin, *J. Comput. Chem.* **2004**, *25*(13), 1605–1612.

- [46] C. P. Konken, G. Haufe, K. Brömmel, B. Wünsch, M. Schäfers, S. Wagner, V. Hugenberg, *Dyes Pigm.* **2018**, *158*, 88–96.
- [47] A. M. Courtis, S. A. Santos, Y. Guan, J. A. Hendricks, B. Ghosh, D. M. Szantai-Kis, S. A. Reis, J. V. Shah, R. Mazitschek, *Bioconjugate Chem.* **2014**, *25*(6), 1043–1051.
- [48] F. Galla, C. Bourgeois, K. Lehmkuhl, D. Schepmann, M. Soeberdt, T. Lotts, C. Abels, S. Ständer, B. Wünsch, *MedChemComm* **2016**, *7*, 317–326.
- [49] V. Butsch, F. Börgel, F. Galla, K. Schwegmann, S. Hermann, M. Schäfers, B. Riemann, B. Wünsch, S. Wagner, *J. Med. Chem.* **2018**, *61*, 4115–4134.
- [50] A. Hascher, A.-K. Haase, K. Hebestreit, C. Rohde, H.-U. Klein, M. Rius, D. Jungen, A. Witten, M. Stoll, I. Schulze, S. Ogawa, R. Wiewrodt, L. Tickenbrock, W. E. Berdel, M. Dugas, N. H. Thoenissen, C. Müller-Tidow, *Clin. Cancer Res.* **2014**, *20*, 814–826.
- [51] G. Jones, P. Willett, R. C. Glen, A. R. Leach, R. Taylor, *J. Mol. Biol.* **1997**, *267*, 727–748.
- [52] D. A. Case, T. A. Darden, T. E. Cheatham III, C. L. Simmerling, L. Wang, R. E. Duke, R. Luo, M. Crowley, R. C. Walker, W. Zhang, K. M. Merz, B. Wang, S. Hayik, A. Roitberg, G. Seabra, I. Kolossváry, K. F. Wong, F. Paesani, J. Vanicek, X. Wu, S. R. Brozell, T. Steinbrecher, H. Gohlke, L. Yang, C. Tan, J. Mongan, V. Hornak, G. Cui, D. H. Mathews, M. G. Seetin, C. Sagui, V. Babin P. A. Kollman, *AMBER 10*, University of California, San Francisco, **2008**.

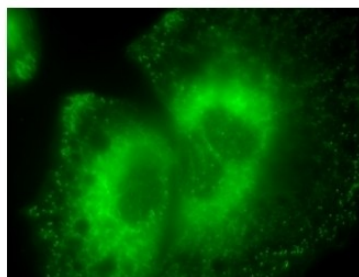
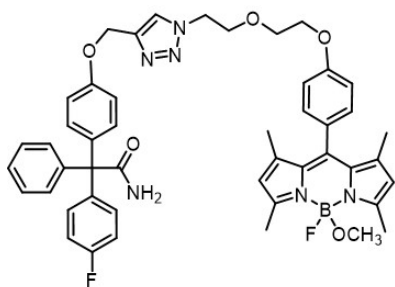
---

Manuscript received: October 10, 2022

Revised manuscript received: October 31, 2022

Accepted manuscript online: October 31, 2022

Version of record online: ■■■, ■■■■



green dot = single  $K_{Ca3.1}$  ion channel

**Highly aggressive human tumors use the  $\text{Ca}^{2+}$  activated  $\text{K}^{+}$  channel  $\text{K}_{\text{Ca}3.1}$  for key processes of the metastatic cascade. Imaging of the  $\text{K}_{\text{Ca}3.1}$  channel *in vitro* and *in vivo* represents a valuable diagnostic and prognostic**

tool. A 18-fluorine labeled senicapoc-based PET tracer showed promising imaging properties *in vivo*. The senicapoc-BODIPY conjugate shown in the figure allowed labeling of single  $K_{Ca}3.1$  channels *in vitro*.

*I. Thale, S. Maskri, L. Grey, L. M. Todesca, Prof. Dr. T. Budde, Dr. I. Maisuls, Prof. Dr. C. A. Strassert, Prof. Dr. O. Koch, Prof. Dr. A. Schwab, Prof. Dr. B. Wünsch\**

1 - 13

## Imaging of K<sub>Ca</sub>3.1 Channels in Tumor Cells with PET and Small-Molecule Fluorescent Probes

